

PAPER • OPEN ACCESS

Azimuthal magnetic field gradient effects on the performance and stability of a 5 kW Hall effect thruster

To cite this article: Chhavi Chhavi and Mitchell L R Walker 2025 *Plasma Sources Sci. Technol.* **34** 115006

View the [article online](#) for updates and enhancements.

You may also like

- [Cracking ammonia in atmospheric-pressure nitrogen microwave discharge plasma to produce hydrogen](#)
Yu-Long Niu, Shou-Zhe Li, Gui-Bin Xu et al.
- [Nanosecond discharges as a tool for measuring energy efficiency \(G-values\) at high reduced electric fields based on nitrogen dissociation](#)
Inna Orel, Youssef Haouchat, Tat Loon Chng et al.
- [Plasma asymmetry effects induced by inter-electrode thermal gradients in capacitively coupled radio frequency plasmas](#)
Xing-Yu Li, Quan-Zhi Zhang, Julian Schulze et al.



HIDEN
ANALYTICAL
Trusted in Research
for over 40 years

www.HidenAnalytical.com

Plasma Diagnostics for Fundamental and Applied Research

Mass & energy analysis of ions, neutrals and radicals



ESPion Advanced Langmuir Probe

- Langmuir probes for plasma diagnostics
- RF compensation
- Multiple configuration options available

Find Solutions for Your Research

Azimuthal magnetic field gradient effects on the performance and stability of a 5 kW Hall effect thruster

Chhavi Chhavi^{1,*}  and Mitchell L R Walker²

Georgia Institute of Technology, Atlanta, GA 30332, United States of America

E-mail: chhavi@gatech.edu and mitchell.walker@ae.gatech.edu

Received 22 April 2025, revised 22 September 2025

Accepted for publication 22 October 2025

Published 13 November 2025



CrossMark

Abstract

Hall effect thruster (HET) component manufacturing defects can result in non-uniformities in the plasma plume, significantly affecting thruster performance. The present work quantifies the effect of an azimuthal magnetic field gradient on the thrust, stability, and efficiency of a 5 kW HET. The study introduces an azimuthal magnetic field gradient inside the discharge channel of the P5, a 5 kW HET, through modifications of the outer magnetic coil circuit to simulate the impact of a manufacturing defect in the magnetic circuit. Far-field plasma probes are utilized to measure plasma properties to compare them to the measured performance. A three-dimensional sweep probe apparatus quantifies the effect of the azimuthal magnetic field gradient on the direction of the thrust vector. The azimuthal magnetic field gradient results in decreased stability during operation. The peak-to-peak discharge current oscillations increase by 31.1%, efficiency decreases by 25.7% and thrust decreases by 3.5% (2.7 mN) due to a 16.6% decrease in the local magnetic field resulting in an extreme gradient condition (0.36 G/°). The sweep probe apparatus observes a 24% decrease in the ion beam current and a 5.8° spatial deviation in the thrust vector for the HET with a 0.36 G/° magnetic field gradient. The study presents a physics-based framework that elucidates the observed patterns in thruster performance caused by variations in plasma characteristics. Through the physics-based performance model proposed in the study, the impact of the azimuthal magnetic field gradient on the electron parameters, such as the electron temperature is established. The impact of the azimuthal magnetic field gradient on HET performance and stability is established in the physics-based model by understanding the impact of such a gradient on the motion of the charged particles by utilizing plasma plume parameters.

Keywords: plasma physics, thruster performance, stability, magnetic field, gradients, Hall effect thruster

¹ Graduate Researcher, School of Aerospace Engineering and AIAA Student Member.

² Professor and Chair, School of Aerospace Engineering and AIAA Fellow.

* Author to whom any correspondence should be addressed.



Original content from this work may be used under the terms of the [Creative Commons Attribution 4.0 licence](https://creativecommons.org/licenses/by/4.0/). Any further distribution of this work must maintain attribution to the author(s) and the title of the work, journal citation and DOI.

1. Introduction

Hall effect thrusters (HETs) are electrostatic devices providing thrust required for operational maneuvers through the acceleration of the ionized propellant particles as they exit the HET channel [1]. HETs are widely used across the space sector [2–4] due to their simple design, strong propulsion, and excellent efficiency. The increasing prevalence of HETs in the commercial sector is a contributing factor to its use as one of the main propulsion systems [5–8]. Contemporary space missions necessitate propulsion units that provide significant thrust and power capability. HETs are employed in two distinct manners to accomplish the mission aim [9, 10]. Integrating mission and mass production requirements increases the probability of manufacturing defects in the HET components, resulting in their inability to complete flight qualification tests effectively. Disparities in plasma [11–13] properties result from the presence of manufacturing defects in various HET components, which consequently alter the performance parameters of the thruster [14]. These inconsistencies may result in a variation in the beam current and its subsequent deviance from the centerline. This can lead to thrust vectoring and modify the plasma parameters and processes. Research has been conducted to determine the relationship between plasma qualities and their impact on HET performance metrics.

Komurasaki and Arakawa [15] investigated the performance and acceleration mechanisms of HETs, employing experimental thrust and beam property measurement techniques. The HET studied by Komurasaki *et al* comprised of standard components found in typical HET systems, including an anode, cathode, and magnetic circuit. Additional assessment of the efficiency of ion acceleration via the constructed model indicated that a rise in both the mass flow rate of the propellant and the acceleration voltage led to a corresponding enhancement in acceleration efficiency. Kim [16] investigated the impact of primary physical characteristics and processes on the performance of SPTs, explicitly focusing on the ionization process and ion dynamics within the channel. The study emphasized the relevance of the magnetic field topology for concentrating ion flow by asserting the function of the magnetic field topology in influencing the electric field structure responsible for ion trajectory variation. The discharge current decreased by 35% as the radial magnetic field gradient increased by 10%. The intricate characteristics of the plasma processes occurring in the HET necessitate the creation of a model that elucidates the electrons and plasma dynamics within the acceleration channel.

Hofer and Jankovsky [17] presented a comprehensive performance model incorporating utilization efficiencies for partially ionized plasma to examine the influence of electron and ion current on thruster performance. The performance model supplied a combination of thruster performance and plasma parameters to calculate properties that are difficult to measure with a probe. The correlations in this study establish a connection between the dynamics of charged particles and plasma properties. The study provided performance parameters as a function of the acceleration voltage or a combination

of the discharge and loss voltage. The model worked effectively for power ranges between 2.16 and 21.60 kW and performed well in multi-charge plasma conditions. The results indicated a relatively high level of accuracy between the model and experimental data, with deviations of less than 5% seen in most cases. Both the modeled calculations and the data gained during testing revealed that increasing the discharge voltage increased the specific impulse and the thruster's efficiency. Despite extensive studies on the correlation between operational parameters (such as mass flow rate and magnetic field) and the impact on ion dynamics and thruster performance, there still needs to be a more comprehensive investigation into the specific effects of magnetic fields on electron dynamics.

The crucial role of the magnetic field in stable HET operation drives the research toward understanding various magnetic field effects that significantly impact HET performance. Magnetic fields are generated using permanent magnets or an inner coil and outer coils in concentric or non-concentric configurations. A conventional HET's magnetic field is axisymmetric to establish uniform plasma generation—the axial magnetic field gradient results in electron mobility variation across the magnetic field in the discharge channel. Axial magnetic field gradients have been extensively researched to provide an understanding of the requirement of the gradient in the magnetic field [18–21]. Morozov *et al* [19] demonstrates the need for a vanishing magnetic field towards the anode to maintain current continuity. The axial gradient of the radial magnetic field ∇B is varied along the discharge chamber centerline from the anode to the thruster exit. The markedly higher electron transport for the negative gradient is attributed to increased plasma oscillations. The uniform gradient provides marginally stable operating conditions; hence, a positive gradient for the magnetic field is essential for stable HET operation. While axial gradient effects are widely studied, radial magnetic field effects in the discharge channel are equally significant. Research has taken place to understand the role of the magnetic field gradient on HET operation [21–23]. Through developing a 2D plasma flow model, Keidar and Boyd [22] established the relationship between the mirror effect and the potential distribution in the HET discharge channel. The research presents that the magnetic field gradient affects important flow characteristics, such as the radial sheath potential drop, the sheath length, and the two-dimensional potential shape in the channel.

Studies on the effects of the axial and radial magnetic field have effectively contributed to establishing the magnetic field's crucial role in HET operation [24–29]. This results in the utmost need to develop a performance model that highlights the relationship of the magnetic field on the thruster performance parameters using plasma parameters to provide a complete understanding of the dependency on the magnetic field. In conventional HET operation, the magnetic field is also considered axisymmetric. However, manufacturing production issues can lead to defects in HET components even if they are within mechanical tolerance, resulting in a non-uniform magnetic field. The non-uniformities in the magnetic field can be observed azimuthally in the channel in

various conditions resulting from electrical shorting, material processing, and geometrical constraints. Numerous studies have been conducted addressing non-uniformities present in HETs. Non-uniformities arise in HETs due to several manufacturing faults, such as non-uniform propellant flow [14], non-uniformities in the propellant neutral density [30], anode orifice configurations [31], and electrical shorts. The non-uniformities present in the HET result in azimuthal variations of plasma properties inside the channel. Lazurenko *et al* [32] performed a computational study of azimuthal non-uniformities in magnetic fields to evaluate the effect of the azimuthal magnetic field gradient. To address the conditions and consequences of a non-axisymmetric magnetic field in HETs, thrust vectoring was considered one of the potential applications of asymmetric magnetic fields. Deviation of the thrust vector for SPT-100 by azimuthal magnetic field asymmetry was simulated by creating eight additional coils and four additional outer poles at 300 V and 4.5 mg s^{-1} anode conditions. Allowing the electron temperature, potential, and number density to be constant and symmetric for inertial wall calculations resulted in a simplified model. The visual evidence obtained through simulation techniques to analyze the distribution of ion flux density and velocity supported the concept of thrust vectoring. Similar experiments were conducted on the PPS-Flex [33], having a configurable magnetic circuit to analyze the potential use of the magnetic field for thrust vectoring. In order to enable the application of magnetic fields for thrust vectoring, the PPS-Flex design underwent modifications by augmenting the quantity of independent magnetic flux circuits, hence deviating from the conventional HET design. As a result, an efficient four-stage construction was developed, utilizing 22 coils to operate the thruster. The experiment involved testing approximately 100 distinct magnetic field configurations with varying lens angles for the magnetic field lines in the PPS-Flex device, which was operating at 250 V and had a discharge current of 4.28 A. The research gave valuable insights into the uniform configuration with the maximal magnetic field near the exit plane, which is the most optimal state of thruster performance. Although the study did not advance in tracking the thrust vector, it provided valuable knowledge of the operation of the thruster.

Gradients in the azimuthal magnetic field are formed due to manufacturing defects, and devices possessing thrust vectoring capabilities provide a platform to explore these magnetic field gradients. This current research drives towards providing knowledge on the impact of the azimuthal magnetic field gradient on a 5 kW HET performance and stability utilizing plasma parameters. In the current study, the azimuthal magnetic field gradient is introduced in the channel of a 5 kW laboratory HET, P5 [34], and performance characterization is performed by operating the thruster in uniform and non-uniform magnetic field configurations comprising an azimuthal magnetic field gradient. The impact of the azimuthal magnetic field gradient on the stability and the precise position of the thruster vector in three-dimensional space is analyzed using various diagnostics to quantify the variations in the plasma properties due to azimuthal gradient change in the magnetic field. Section 2 describes a physics-based model that

enables an understanding of the impact of the azimuthal magnetic field gradient on the motion of charged particles, influencing the plasma parameters. Section 3 outlines the experimental setup employed to assess the relationship between the performance parameters and gradients in the azimuthal magnetic field, as established by the model, and demonstrates the model's validity. The results of the various diagnostics that analyze the thruster performance parameters and the various plasma parameters when the thruster is operated at different magnetic field configurations because of the azimuthal magnetic field gradient are discussed in section 4. Lastly, section 5 explains how the azimuthal magnetic field gradient affects the thruster performance parameters by influencing the velocity of charged particles, as demonstrated by effects on plasma properties.

2. Physics-based performance model

2.1. Azimuthal magnetic field gradient effect on electron motion

The previous models, which assume a uniform magnetic field in the HET channel, required significant enhancement to understand magnetic field effects. The purpose of this modification is to develop a model that can be used to thoroughly investigate the impact of an azimuthal magnetic gradient on the plasma parameters that directly influence HET performance. The channel's azimuthal gradient enables the modification of properties in both the radial and axial directions. These gradients result in a complex, three-dimensional problem that is exceedingly difficult to resolve. Consequently, it is necessary to make critical assumptions to facilitate the development of the model and establish a correlation between the azimuthal gradient magnitude and the thruster performance parameters. The present model is based on the following assumptions. 1) The focus is solely on the azimuthal gradient, disregarding the radial gradient that is present in the channel. 2) Ignoring the wall interactions, resulting in energy losses as a consequence of recombination and electron emission. 3) Developing the model at the maximal magnetic field region near the exit plane and disregarding the gradient in the axial direction.

During the examination of the specific area of interest in the channel, it is divided into two distinct regions. As depicted in figure 1, region one denotes a uniform magnetic field with a high magnitude. In contrast, region two indicates where the magnetic field is decreased to establish an azimuthal magnetic field gradient within the channel between regions one and two. A detailed look at the area shows that electrons move from region one to two, providing a clear visual of the area of focus.

The velocity of the electrons in the region can be expressed as a sum of the velocity imparted to the electron along the magnetic field, \vec{v}_{\parallel} and the $E \times B$ drift velocity caused by the Lorentz force resulting from the presence of perpendicular electric and magnetic fields in the channel, $\vec{v}_{(E \times B)}$ as shown in equations (1) and (2). Where \vec{v}_e represents the average electron velocity, m_e is mass of electron, B_r is radial component of the magnetic field, e denoting electron charge, r_L is Larmor radius, E_z represents the axial component of the electric field,

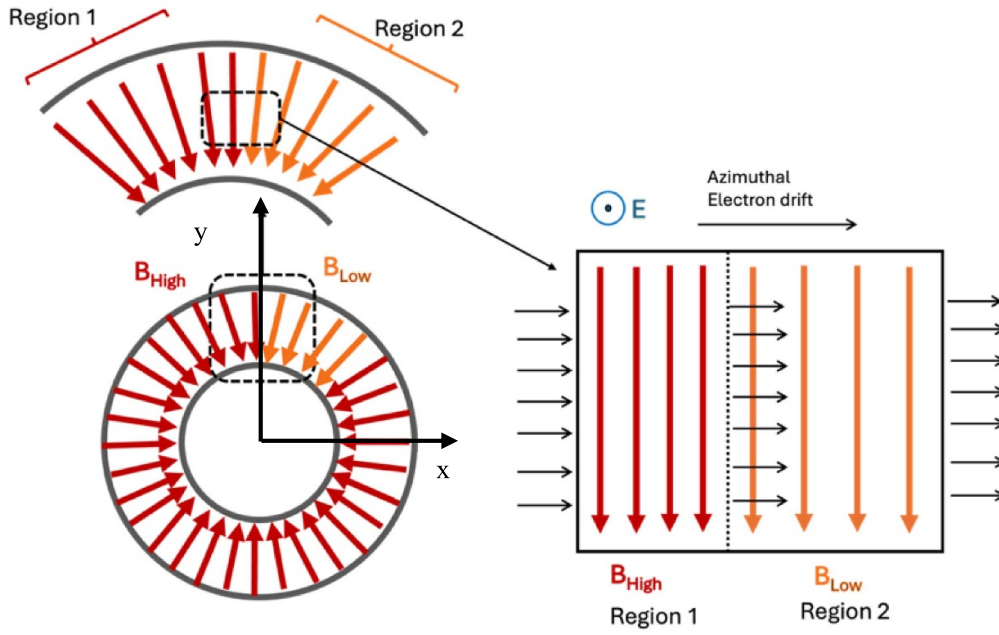


Figure 1. Azimuthal electron drift motion direction (x) in the presence of an azimuthal magnetic field gradient.

ν_e is the electron collision frequency, n_e is the electron number density, v_{e_z} represents electron velocity in z direction and $j_{e\theta}$ is angular electron current density,

$$\vec{v}_e = \vec{v}_\perp + \vec{v}_{(ExB)} \quad (1)$$

$$v_e = \frac{eB_r r_L}{m_e} + \frac{E_z}{B_r} \quad (2)$$

$$\nu_e n_e v_{e_z} m_e + q n_e E_z + j_{e\theta} B_r + \frac{dp}{dz} = 0 \quad (3)$$

As the magnetic field shifts from one location to another, the velocity along the magnetic field lines is balanced by the potential gradient in the radial direction. Therefore, no magnetic field impact is observed in the first term representing the motion along the magnetic field line. Since we are investigating the influence of the gradient in the azimuthal direction represented by x in figure 1, Hofer's performance model [17] is utilized to discuss the effect of introducing the azimuthal gradient on the drift velocity component associated with the electron. The 1-d steady-state momentum equation demonstrated in equation (3) provides a suitable starting point for investigating the effects of the azimuthal velocity gradient due to magnetic field, on the plasma properties and HET performance while maintaining the same assumptions as the performance model developed by Hofer and Jankovsky [17]. The modification of equation (3) for the azimuthal direction, along with a comparison with equation (3), establishes a relationship between the axial current density and the azimuthal current density that can be translated into an axial, v_{e_z} and azimuthal velocity, v_{e_x} relation through the electron Hall parameter, Ω_e shown in equation (4). It is crucial to note that the

cartesian coordinate system is used to build the solution rather than the radial coordinate system for ease of use. The scaling laws established for the HET facilitate the scaling of the HET by preserving the ratio between its radius and length to provide analogous performance characteristics [35]. A constant ratio of radius-to-length facilitates a correlation between the radial dimension and the axial dimension of the thruster. In the current research work's coordinate system, the dimensions x and z may be regarded as dependent variables, hence maintaining the interdependence between the radial and axial dimensions of the thruster. For the current model for a section of the channel, the azimuthal direction is in cartesian coordinates and represented with variable x along with z variable representing the axial direction as shown in figure 1.

$$v_{e_x} = v_{e_z} \Omega_e \quad (4)$$

Using equations (3) and (4), the axial current density, j_{e_z} is estimated to be influenced by axial mobility, the electric field, E_z and the pressure effects, p as shown in equation (5),

$$j_{e_z} = \mu_{e_z} \left(-en_e E_z - \frac{dp}{dz} \right). \quad (5)$$

Equation (5) can be written for the azimuthal current density, j_{e_x} as

$$j_{e_x} = \mu_{e_x} \Omega_e \left(-en_e E_z - \frac{dp}{dz} \right) \quad (6)$$

$$j_{e_x} = \mu_{e_x} \left(-en_e E_z - \frac{dp}{dz} \right). \quad (7)$$

The azimuthal mobility, μ_{e_x} is expressed as the sum of the axial mobility, μ_{e_z} and the Hall parameter as shown in equation (8). It is utilized to establish the connection between the azimuthal drift velocity of electrons and the azimuthal magnetic field gradient within the channel,

$$\mu_{e_x} = \mu_{e_z} \Omega_e. \quad (8)$$

Thus, the azimuthal velocity of electrons from equation (4) can be written as

$$v_{e_x} = \mu_{e_x} \left(-E_z - \left(\frac{1}{en_e} \right) \frac{dp}{dz} \right) \quad (9)$$

$$p = n_e k T_e \quad (10)$$

$$v_{e_x} = \mu_{e_x} \left(-E_z - \left(\frac{k}{en_e} \right) \frac{d(n_e T_e)}{dz} \right). \quad (11)$$

Where k is Boltzmann constant and T_e is the electron temperature. To estimate the changes in the azimuthal direction due to the azimuthal magnetic field gradient, the gradient in velocity is estimated by using equation (11),

$$\frac{dv_{e_x}}{dx} = \frac{d\mu_{e_x}}{dx} \left(-E_z - \left(\frac{k}{en_e} \right) \frac{d(n_e T_e)}{dz} \right) - \mu_{e_x} \frac{d}{dx} \left(\frac{k}{en_e} \right) \frac{d(n_e T_e)}{dz} \quad (12)$$

$$\frac{dv_{e_x}}{dx} = \frac{d\mu_{e_x}}{dx} \frac{v_{e_x}}{\mu_{e_x}} - \mu_{e_x} \frac{d}{dx} \left(\frac{k}{en_e} \right) \frac{d(n_e T_e)}{dz}. \quad (13)$$

The gradient in the azimuthal mobility with position can be determined using the relation presented in equation (13). As mentioned above, the x and z are considered as dependent variables due to the scaling laws used in the industry to establish a relationship between axial and radial relations. The positional gradient is determined by the alterations in the Hall parameters caused by the azimuthal fluctuations in the magnitude of the magnetic field,

$$\mu_{e_x} = \Omega_e \frac{e}{m_e \nu_e (1 + \Omega_e^2)} \quad (14)$$

$$\frac{d\mu_{e_x}}{dx} = \frac{d}{dx} \Omega_e \frac{e}{m_e \nu_e (1 + \Omega_e^2)} \quad (15)$$

$$\frac{d\mu_{e_x}}{dx} \approx \frac{d}{dx} \left(\frac{1}{B_r} \right). \quad (16)$$

In order to simplify the equation, the pressure effects are ignored to determine the changes in velocity neglecting the thermal motion change,

$$\frac{dv_{e_x}}{dx} = - \frac{d\mu_{e_x}}{dx} \left(E_z + \left(\frac{k}{en_e} \right) \frac{d(n_e T_e)}{dz} \right) \quad (17)$$

$$\frac{dv_{e_x}}{dx} \propto \left(- \frac{d}{dx} \left(\frac{1}{B_r} \right) \right). \quad (18)$$

As the electron moves from region one to region two, the magnetic field decreases across the boundary, resulting in a negative azimuthal gradient in the magnetic field. This negative gradient increases the azimuthal drift velocity of electrons from regions one to two, as per equation (18). According to equation (4), changes in the azimuthal drift velocity can cause variations in the axial velocity of the electrons,

$$\frac{dv_{e_z}}{dx} = \frac{1}{\Omega_e} \left(\frac{dv_{e_x}}{dx} - v_{e_z} \frac{d\Omega_e}{dx} \right) \quad (19)$$

$$\frac{d\Omega_e}{dx} = \frac{d}{dx} \left(\frac{eB}{m_e \nu_e} \right). \quad (20)$$

Due to the negative gradient introduced in the channel, the electron's axial velocity increases as they traverse region one to region two. Therefore, the azimuthal magnetic field gradient in the HET channel can influence the axial motion of electrons, leading to modifications in the plasma parameters. The electron's temperature does not increase to the same extent as in the presence of a uniform magnetic field, thus decreasing the electron's overall temperature. The electron interactions that lead to ionization are diminished due to the electron's lower total energy, which is insufficient for collisions to induce ionization. The ionization region in the azimuthal gradient region shifts locally upstream towards the anode in comparison to the region where a uniform magnetic field is present as a result of the increase in the axial velocity of the electrons due to the presence of the azimuthal gradient in the channel as seen in figure 2. This localized shift in the location of the ionization region results in an increase in the length of the acceleration region at that location, which in turn causes non-uniformities in the axial location of the ionization acceleration region in the channel. The voltage loss increases as the ionization region moves upstream at the gradient location, resulting in the ions being lost to the wall rather than being accelerated out of the channel. Therefore, the rise in voltage loss reduces the overall acceleration voltage experienced by the ion particle. The decrease in the available acceleration voltage leads to a decrease in the ion velocity, affecting the thruster's performance due to a gradient in the azimuthal magnetic field.

2.2. Hall thruster performance model

Hofer [14] established a correlation between the thruster performance and plasma parameters presented by equation (21)–(24), where A is the cross sectional area of discharge channel \dot{m}_a is the anode mass flow rate, n_i is the ion number density and $i\dot{m}_b$ the ion beam mass flow rate. Yamamoto *et al* [36] defines stability as the ratio of the root-mean-square of discharge current oscillations to the discharge current observed under power conditions. This ratio, as seen in equation 26, is utilized to observe the effect of the magnetic field on the HET stability and is considered one of the stability parameters to observe during experimentation. Along with the ratio of root-mean-square of the discharge current oscillations to the discharge current, I_d the magnitude of the discharge current oscillation, as measured by the peak-to-peak oscillation percentage,

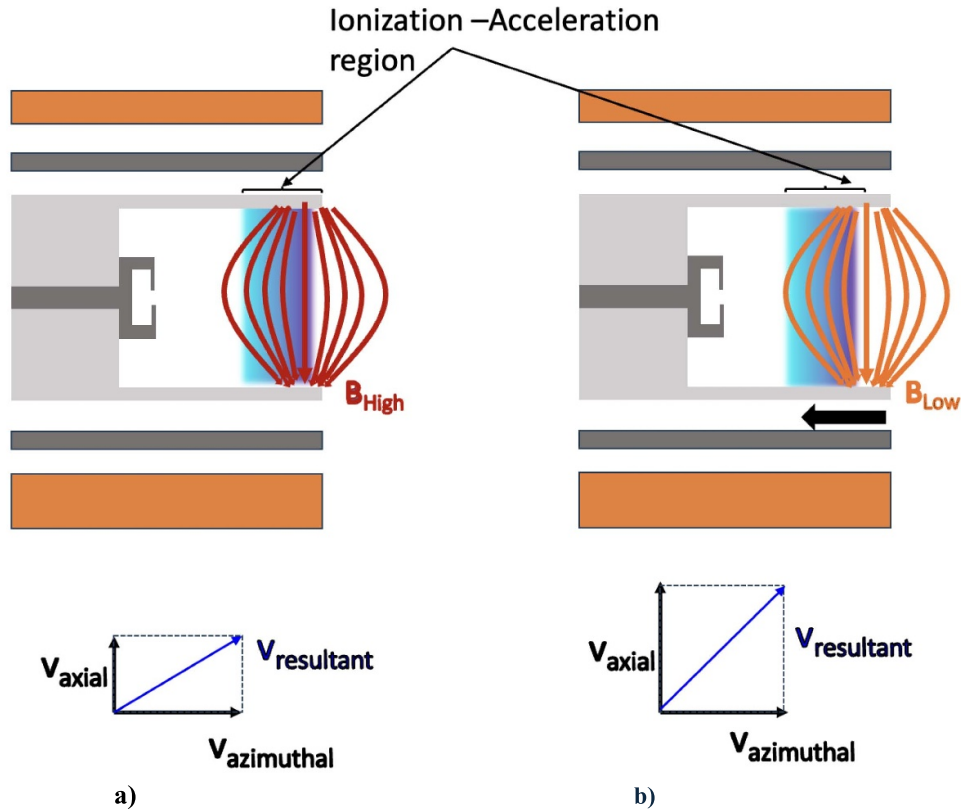


Figure 2. Schematic of displacement of the ionization-acceleration region as well as the resultant electron velocity vector in the (a) high magnetic field region and (b) low magnetic field region.

is also considered a critical indicator of stability with changes in the magnetic field. The peak-to-peak oscillation percentage is considered a primary indicator of stability for the current study.

Introducing a gradient in the channel leads to an overall increase in the electron velocity, increasing the discharge current. A reduction in the ion velocity, v_b and acceleration voltage, V_a leads to an overall decrease in the ion beam current, I_b . Introducing the gradient in the channel contributes to the overall decrease in the current utilization efficiency, η_b as the discharge current, I_d and ion beam current fluctuate. The variations in the ion velocity also contribute to a reduction in the thrust, T and specific impulse, I_{sp} that the ion imparts at the thruster operating configuration. The reduction in the acceleration voltage, V_a leads to a corresponding decrease in the voltage utilization efficiency, η_v . The stability equations established by Yamamoto *et al* [36] play a crucial role in predicting the thruster's operation state. For instance, when the axial electron velocity increases, the second component of the equation (25) becomes more negative. This reduction leads to a drop in overall stability, causing the thruster to operate in an unstable state,

$$\eta_b = \frac{I_b}{I_d} = \frac{n_i e v_b A}{n_i e v_i A - n_e e v_e A} \quad (21)$$

$$\eta_v = \frac{V_a}{V_d} \quad (22)$$

$$T = \dot{m}_b v_b \quad (23)$$

$$I_{sp} = \frac{T}{\dot{m}_a g} \quad (24)$$

$$(A v_e)_{\text{exit}} - (A v_e)_{\text{anode}} - (\sigma_{d_i} \vartheta_e)_{T_e} > 0 \quad (25)$$

$$\Delta = \frac{I_{d,\text{rms}}}{I_d} = \frac{1}{I_d} \sqrt{\int_0^\tau (I_d - \bar{I}_d) dt} \quad (26)$$

The background knowledge of the variations in the plasma properties as the gradient is introduced is provided by the relationships established by the model to analyze the effect of introducing an azimuthal magnetic field gradient, which in turn affects the thruster performance parameters. While the model requires further development to incorporate three dimensional effects, it provides a good base for understanding the potential impact of the azimuthal magnetic field gradient on mid-power thruster performance and stability. An experimental test campaign is conducted on a 5 kW HET to substantiate the established relationships and observe the effects on thruster performance as well as stability. The experiment involves the introduction of an azimuthal magnetic field gradient of varying magnitudes into the channel, and the effect of this gradient is observed on the thruster performance and plasma parameters.

3. Experimental procedure

3.1. Vacuum test facility: VTF-2

The VTF-2 consists of a 9.2 m long stainless-steel vacuum chamber with a diameter of 4.9 m that attains high vacuum using ten liquid nitrogen-cooled CVI TM1200i cryopumps linked to two Stirling Cryogenics SPC-4 compressors [37]. Agilent Bayard–Alpert (BA) 571 hot-filament ion gauges on the chamber flange, along with MKS Granville Phillips 370 Stabil-ion gauges located 0.3 m downstream of the exit plane and 0.6 m from the thruster centerline, were used to measure pressure. The ion gauges were regulated to deliver precise pressure measurements using different controllers; the Agilent XGS-600 Gauge Controller controls the outer ion gauge, and the Granville Phillips 370 Controller controls the ion gauge inside the chamber. Nominal operating pressures of 5.9×10^{-6} Torr- N_2 and 1.1×10^{-5} Torr- N_2 are observed inside the chamber. The average operational and base pressures were measured using the outer and inner gauges. Subsequently, the operational pressure was adjusted for krypton using a correction method

$$p_{\text{Operational-corrected}} = 1/\text{corr}(p_{\text{Operational-measured}} - p_{\text{base}}) + p_{\text{base}}, \quad (27)$$

with corr being equal to 1.96 for krypton [38]. During operation, the base and operational pressure in the facility were maintained at 2.55×10^{-9} Torr- N_2 and 3.1×10^{-6} Torr-Kr.

3.2. 5 kW Hall thruster

The 5 kW laboratory P5 HET, built in 1997 through a collaboration between Ron Spores of the Air Force Research Laboratory (AFRL) and Alec Gallimore of the University of Michigan, is used as the test subject for conducting the experiment. A detailed discussion regarding the thruster is provided by Gulczinski [34]. Distinct features of P5 include 36 slotted holes in the stainless-steel anode, a ceramic discharge channel, an inner magnetic core, and eight outer magnetic cores constituting the magnetic circuit of the thruster. The thruster comprises a boron nitride and silicon dioxide BN-SiO₂, M26 grade channel with an outer diameter of 173 mm and a width of 25 mm [25, 39]. EPL-500, a hollow cathode is situated at the -35° vertical position with respect to the thruster centerline at a distance of 2.2 cm downstream of the P5 exit plane and 7 cm above the centerline. Operation of the thruster for the current study is conducted at a discharge voltage of 300 V, an anode flow rate of 5.61 mg s^{-1} of krypton, and a cathode flow rate of 0.44 mg s^{-1} of krypton. In order to introduce a magnetic field gradient to evaluate the effect of non-uniformities in the magnetic field on the ion beam current and the thrust vector, the outer magnetic circuit is split into three sections. The splitting of the outer magnetic circuit provides control of the current supplied to the thruster's outer magnetic coil circuit, thus allowing the magnetic field magnitude to vary azimuthally across the channel. The outer magnetic circuit is split to operate two coils independently (OC2 and OC3), while the other six coils are connected in series to be operated using a TDK

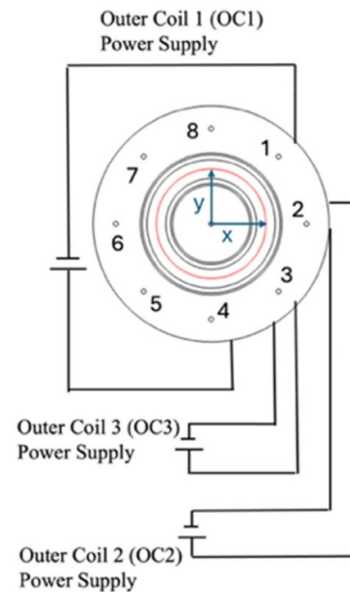


Figure 3. Schematic of P5 outer magnetic circuit.

Lambda power supply (OC1). A FW Bell Gaussmeter 5080 was utilized to measure the magnetic field in the thruster channel. Figure 3 shows a schematic representation of the setup.

3.3. Diagnostics

The diagnostics employed to quantify various plasma parameters included a sweep probe apparatus, Langmuir probe, retarding potential analyzer (RPA), oscilloscope, and inverted pendulum thrust stand. The sweep probe apparatus, Faraday probe, Langmuir probe, and RPA are mounted on a radial arm driven by a Parker Daedal 200RT rotary motion stage and positioned 1 m from the thruster output plane, and the oscilloscope is connected to the discharge circuit in the control room.

1. Three-dimensional sweep probe apparatus

The apparatus consists of a circular framework with a radius of 1 meter, constructed from lightweight aluminum, as depicted in figure 4. The framework comprises a geared track on one side and a curved flat surface insulated from the plume using graphite fragments on the other side. A slot is created in the aluminum structure to accommodate motion bearings and preserve the orthogonality of the probe while moving along a curved trajectory. The bearing linked to the probe mount guarantees that the probe remains in the correct orientation while sweeping through the plume. The geared track framework ranges from -41° to 46° , providing a measurement span of 87° of the plume. The framework can be extended to a 180° span in facilities without spatial restrictions such as the floor and the thruster mount. The probe mount is fabricated utilizing a combination of aluminum and graphite components. The aluminum brackets are connected to the motion gear, and the stepper motor is employed for motion control. A Nema 17 motor with a 50:1 ratio planetary gearbox is utilized to translate the probe along a 1 m radius path via a motion gear with a step size of 1.8° per step.

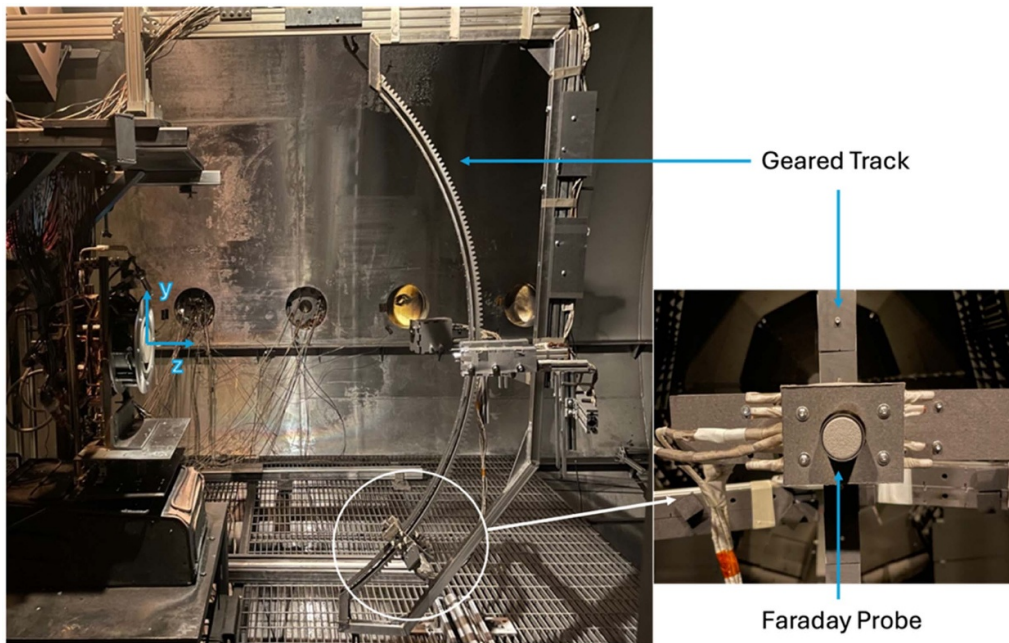


Figure 4. Picture of the 1 m curved sweep probe apparatus installed in VTF-2.

A stepper motor is employed with limit switches positioned at the endpoints to monitor the probe's location as it moves along a curved path. At -45° and 50° from the track, high-precision limit switches are arranged so that the probe mount contact can activate the limit switch circuit and halt the stepper's motion. The entire sweep probe apparatus [40] is positioned on a radial probe arm, so there is a 1 m distance between the probe collector and the thruster exit plane in VTF-2, as seen in 6. The radial probe arm is designed to undergo a sweeping motion, starting from -90° and ending at 90° with a velocity of 0.63° per second. The probe arm is controlled by a Parker Daedal 200RT series rotary table, which has an accuracy of $\pm 17^\circ$ [41], as depicted in figure 5. The angular transverse motion and the stepper motor-driven vertical motion of the Faraday probe are controlled by the Agilent 34970 A data acquisition unit. The construction of the Faraday probe adheres to the recommended principles, utilizing a stainless steel casing that is 1 inch in length and a collector coated with tungsten [42]. The collector and guard ring of the Faraday probe are biased at -30 V relative to the ground using a Keithley 2470 source meter. LabVIEW Virtual Instrument records the probe location and the ion beam current gathered by the Faraday probe. Using the Faraday probe, the sweep probe apparatus [40] maps the ion current density distribution.

2. Langmuir probe

The Langmuir probe is used to measure the plasma potential, V_p , the floating potential, V_f , the electron number density, n_e , and the electron temperature, T_e [43]. An alumina ceramic tube measuring 6.4 mm in diameter and 65 mm in length encases a 6.4 mm long tungsten tip of 0.13 mm diameter in the Langmuir probe design. The Langmuir probe is positioned on the radial arm so that the tungsten electrode points toward

the thruster. A Keithley 2470 source meter biases the probe from -50 V to $+60$ V, in 0.1 V increments, with respect to ground, and measures the current. The current is collected at the centerline of the thruster at an angular position of 0° with respect to the thruster plume center through three consecutive voltage sweeps and analyzed using classical thin sheath theory [43]. In order to obtain accurate ion density and temperature measurements, the classical thin sheath theory is applied which states that the impact of sheath thickness is negligible in comparison to the probe radius. A LabView program records the Keithley 2470 data output.

3. RPA Probe

The RPA is used to quantify the ion energy distribution within the thruster plume [44]. The RPAs consist of four grids: the floating grid, the electron repulsion grid, the ion repulsion grid, and the electron suppression grid. The floating grid is oriented to face the plasma plume. In order to protect the plasma from the perturbations caused by the probe's presence, the floating grid is permitted to float electrically. The electron repulsion and suppression grid are biased to -30 V relative to the ground to prevent plasma electrons and high-energy secondary electrons from reaching the collector. A Keithley 2470 source meter measures the ion current as a function of the ion repulsion grid repelling voltage. The ion repulsion grid is scanned with a bias voltage ranging from 0 to 450 V, with a voltage spacing of 2 V relative to the ground. Post-processing of the ion current as a function of repelling voltage, corrected for the plasma potential, yields the ion energy distribution function. Three successive voltage sweeps are conducted to account for the uncertainty and variability in data. The voltage measurement of the RPA, V_{rpa} for the ion energy distribution peak between scans exhibited a variability of $\pm 5\%$. The RPA is affixed to the radial arm to obtain a measurement

of the centerline location with a 0° angular position about the thruster plume.

4. Oscilloscope

A high-definition, four-channel oscilloscope was employed to capture time-resolved measurements of the P5 discharge current. The time-resolved measurements for the discharge current I_d , the peak-to-peak variation of the discharge current $I_{d,pk2pk}$, and the root mean square measurement of the discharge current $I_{d,rms}$ were captured using a Teledyne LeCroy HDO6104A oscilloscope. This oscilloscope has a DC—1 GHz bandwidth and a resolution of 12 bits. The oscilloscope was configured with a time base of ± 5 ms and a sampling rate of 50 MS s^{-1} , with a maximum discernible frequency of 20 MHz. The characteristics of the discharge current oscillations were measured using a Teledyne LeCroy CP150 current instrument. The CP150 has a maximum rated current of 300 A and a DC—10 MHz bandwidth. In order to monitor the oscillations generated by the HET plume, the CP150 sensor was installed at the power feedthrough that corresponds to the anode power line upstream of the RC filter. The average values of the discharge current characteristics across the five traces were determined by capturing a minimum of five oscilloscope traces for the HET discharge at each operating condition. The power spectral density was obtained by performing a fast Fourier transform on the time-resolved discharge current. The peak frequency was $6.4 \text{ kHz} \pm 900 \text{ Hz}$. The peak frequency exhibited a magnitude shift of 2 kHz under the non-uniform test conditions. It is crucial to notice that, despite a gradient in the channel, the oscillations' peak frequency remains below the frequently observed breathing mode instability, which ranges from 10 to 30 kHz. Consequently, the present investigation does not examine breathing mode instabilities but local plasma low-frequency instabilities.

5. Inverted pendulum thrust stand

A null-type, water-cooled, inverted pendulum thrust stand is employed to measure thrust based on the thrust stand design developed by the NASA Glenn Research Center [25]. The thrust stand is composed of a pair of parallel plates connected by a series of four flexures. These flexures support the upper plate and allow it to deflect in response to an applied force. The upper plate's position is monitored by a linear voltage differential transformer (LVDT) and regulated by two electromagnetic actuators. During operation, a pair of SIM 960 analog proportional-integral-derivative controllers regulate the current through each actuator by modulating the current through the actuators based on the LVDT signal. This process eliminates any vibrational noise (damper coil) and keeps the upper plate stationary (null coil). The current through the null coil, necessary to maintain the upper plate's stationary position, is directly proportional to the thrust. The thrust stand is actively water-cooled to facilitate the chilling of the null coil circuit during thruster firings in order to preserve thermal equilibrium. An 1100-W VWR International 1173-P refrigerated recirculation chiller supplies the cooling water, which does not fluctuate by more than 5°C compared to the thruster-off condition.

The thrust stand is calibrated by employing a collection of weights that are well-known and cover the entire range of anticipated thrust values. In order to provide a measurement of the thrust at an operating condition, a linear fit is established by correlating the null coil current to the force applied to the thrust stand. The thruster was turned off for each of the three consecutive thrust measurements. Following the calibration, the thruster was reactivated, and a thermal steady state was achieved by allowing a change in temperature of less than $\pm 0.5^\circ \text{C}/\text{min}$ before the subsequent set of measurements. This study's average thrust stand uncertainty was approximately $\pm 2 \text{ mN}$ (2.6% full scale), defined as the variability associated with the calibrations conducted for each scan at an operating condition.

4. Results

This section provides the results obtained for the plasma parameters as well as the performance parameters while operating the P5 thruster in uniform and non-uniform magnetic field conditions. The non-uniform magnetic field condition was employed to facilitate the presence of an azimuthal gradient in the magnetic field across the channel. The P5 thruster was powered by a voltage of 300 V, with the outer coil circuits (OC1, OC2, and OC3) and inner coil current set to 4 A and 6 A, respectively. The thruster is operated for three hours at uniform baseline conditions before reaching a thermal steady state displayed by a rate of change of thruster temperature of less than $0.5^\circ \text{C min}^{-1}$. After the thruster reaches a thermal steady state, three-dimensional measurements of the ion beam current using the hemispherical apparatus, with three angular vertical sweeps of the Faraday probe at every 5° horizontal position, are performed to eliminate any systematic inaccuracy caused by the motion control system. Characterization of the ion beam current for the uniform magnetic field configuration provides the baseline condition for comparison with non-uniform conditions to analyze the effect of the magnetic field non-uniformities. After the ion beam current measurement, the Langmuir and RPA mounted on the radial arm are positioned at the centerline for plasma property measurement. Five oscilloscope measurements are noted down for stability estimation through discharge current peak-to-peak measurements. Thrust measurements using the inverted pendulum thrust stand are conducted at the end of each test condition. The mass flow of 5.61 mg s^{-1} and 0.44 mg s^{-1} for the anode and cathode, as well as the discharge voltage of 300 V, are kept constant throughout the study to allow for only magnetic field variation impact of plasma parameters.

Table 1 shows the test matrix commences by reducing the current in coil circuit 2 (OC2) by 50%, resulting in a 5.51% decrease in the magnetic field in the localized area, B_l shown in figure 3. The localized magnetic field was measured using a FW Bell Gaussmeter 5080 for the different magnetic field configurations before the commencement of the test. Magnetic field measurement across the channel using a gaussmeter provided an estimation for the localized magnetic field changes due to the current variations across the outer

Table 1. Operating conditions of P5 for azimuthal magnetic field gradient configurations at 300 V, anode flow of 5.61 mg s^{-1} and cathode flow of 0.44 mg s^{-1} krypton. Test condition 2 or gradient 2 represents the ‘one coil off’ operating condition and test condition 4 or gradient 4 represents ‘two coils off’ operating condition.

Test No.	Condition name	V_d (V)	I_d (A)	B_l (G)	$\nabla_{\theta} B_r$ (G/\circ)	IC current (A)	OC1 Current (A)	OC2 Current (A)	OC3 Current (A)
0	Baseline	300	7.90	145	0.00	6.00	4.00	4.00	4.00
1	Gradient 1	300	7.91	136	0.18	5.85	3.90	2.00	4.00
2	Gradient 2	300	7.94	130	0.31	5.70	3.80	0.00	4.00
3	Gradient 3	300	7.94	125	0.30	5.55	3.70	0.00	2.29
4	Gradient 4	300	8.05	120	0.36	5.40	3.60	0.00	0.00

Table 2. Plasma parameters of P5 for azimuthal magnetic field gradient configurations at 300 V, anode flow of 5.61 mg s^{-1} and cathode flow of 0.44 mg s^{-1} krypton. Test condition 2 or gradient 2 represents the ‘one coil off’ operating condition and test condition 4 or gradient 4 represents ‘two coils off’ operating condition.

Test No.	Condition Name	B_l (G)	$\nabla_{\theta} B_r$ (G/\circ)	I_d (A)	I_b (A)	T_e (eV)	V_p (V)	V_{ppa} (V)	$I_{d,pk2pk}$ (A)	T (mN)
0	Baseline	145	0.00	7.90	5.71	4.27	14.9	270	4.15	78.0
1	Gradient 1	137	0.18	7.91	4.29	3.92	14.6	251	4.11	76.0
2	Gradient 2	131	0.31	7.94	4.40	3.93	14.5	257	5.01	75.6
3	Gradient 3	125	0.30	7.94	4.35	3.85	14.1	254	5.11	75.9
4	Gradient 4	121	0.36	8.05	4.33	3.72	13.9	254	5.32	74.3

magnetic field circuit. The subsequent operating condition entails a reduction in the current in the coil circuit from 2 A to 0 A, which leads to a localized reduction in the magnetic field by 9.65% and an azimuthal gradient, $\nabla_{\theta} B_r$ of $0.18 \text{ G}/\circ$. The test condition 2 or gradient 2 with 0 A current in coil 2 is one of the primary points of the study. The subsequent condition (test condition 3 or gradient 3) necessitated a 50% reduction in coil current in the coil circuit 3 (OC3) and the complete shutdown of the coil 2 circuit. This operating situation leads to an augmentation in the gradient and the length of the specific region undergoing the alteration in the magnetic field. The third operating state is a 13.8% reduction in the magnetic field. The final operating condition (test condition 4 or gradient 4) in test matrix 2 is the complete powering off of outer coil circuit two (OC2) and outer coil circuit three (OC3), enabling only the outer coil circuit one (OC1) to be operational. A gradient of $0.36 \text{ G}/\circ$ and a reduction in the magnetic field by 16.5% are the outcomes of this extreme condition for the current research. At each testing condition, measurements of plasma parameters are conducted using diagnostics used to establish the baseline uniform magnetic field condition. Comparison of the properties allows for the observation of the change in plasma properties due to the introduction of the azimuthal magnetic field gradient.

Table 2 provides values of plasma parameters obtained through the diagnostic measurements conducted for each test condition. Transitioning from the uniform magnetic field test condition to the non-uniform magnetic field condition, a decrease in the localized magnetic field in the area of introduction of the azimuthal gradient by 9.65% for the ‘one coil-off’ condition i.e. test condition 2 or gradient 2 resulted in an 8% decrease in the electron temperature, T_e with a 2.2% decrease in the plasma potential V_p and a 20.7% increase in the discharge current peak to peak, $I_{d,pk2pk}$. ‘Two coil-off’ conditions i.e. test condition 4 or gradient 4 resulted in a 16.55% decrease

in the localized magnetic field, resulting in a 12.8% decrease in the electron temperature T_e , a 6.2% decrease in the plasma potential, and a 28.2% increase in the peak-to-peak of the discharge current. Observing the changes in ion beam current, a 23% decrease is observed for the ‘one coil-off’ condition, whereas ‘two coil-off’ conditions resulted in a 24.2% decrease in the ion beam current.

5. Discussion

5.1. Performance parameters variation due to azimuthal magnetic field gradient

This section provides an evaluation of various magnetic field configurations demonstrating the significant influence of the magnetic field on the performance of the HET. The performance of the HET in the presence of the azimuthal magnetic field gradient is compared with the uniform magnetic field operating condition. The impact of the azimuthal magnetic field gradient on the plasma parameters is discussed to provide a deep understanding of the performance parameters and the observed azimuthal magnetic field gradient as established in the model developed in section 2

Deviation from the optimal operating conditions reduced the performance and operation of the P5 thruster. To quantify the change in HET performance caused by an azimuthal magnetic field gradient, an azimuthal magnetic field gradient was intentionally introduced into the channel. The alteration in the current flow to the OC2 and OC3 coil circuits, which operated independently, facilitated the introduction of a magnetic field gradient in the channel. Table 3 presents the observed performance of the thruster under the baseline condition and four different operating conditions with varying magnitudes of the azimuthal magnetic field gradient. The four test scenarios range in the amount of current provided to the coils,

Table 3. Performance parameters of P5 for azimuthal magnetic field gradient configurations at 300 V, anode flow of 5.61 mg s^{-1} and cathode flow of 0.44 mg/s krypton. Test condition 2 or gradient 2 represents the ‘one coil off’ operating condition and test condition 4 or gradient 4 represents ‘two coils off’ operating condition.

Test no.	Condition name	B_l (G)	$\nabla_{\theta} B_r$ (G°)	T (mN)	I_{sp} (s)	$I_{d,pk2pk}$ (%)	η_b (%)	η_v (%)	η_m (%)	η (%)
0	Baseline	145	0.00	78.0	1410	52.5	52.1	84.9	59.6	22.9
1	Gradient 1	137	0.18	77.0	1392	72.4	50.8	83.9	59.1	21.9
2	Gradient 2	131	0.31	76.8	1387	74.5	50.3	84.1	58.6	21.8
3	Gradient 3	125	0.30	76.6	1384	69.0	50.8	83.9	59.0	21.8
4	Gradient 4	121	0.36	76.5	1382	77.1	49.5	83.9	58.3	21.4

resulting in variations in thrust T , current utilization efficiency η_b , voltage utilization efficiency η_v , mass utilization efficiency η_m , anode efficiency η and percentage of peak-to-peak discharge current oscillation, $I_{d,pk2pk}$.

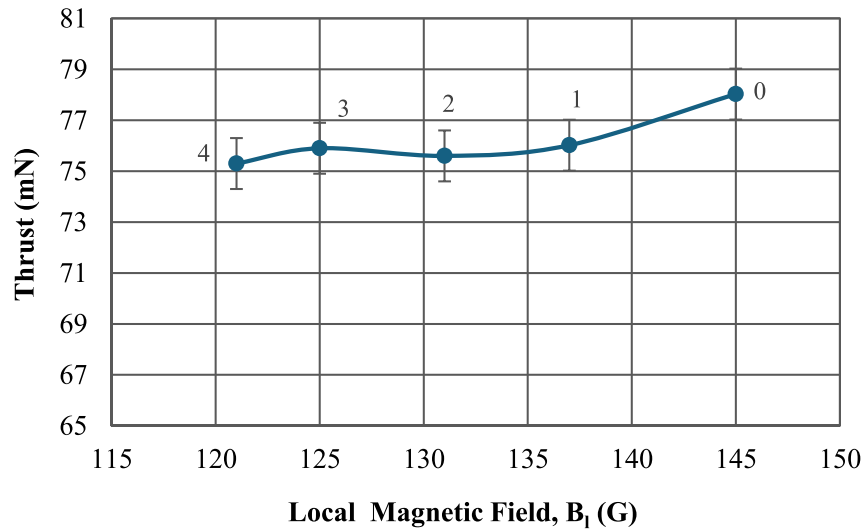
The baseline condition with a uniform magnetic field for P5 was 300 V and 7.92 A, with a cathode mass flow of 5.61 mg s^{-1} and a cathode mass flow of 0.44 mg s^{-1} of krypton. The magnetic circuit configuration consisted of 6 A for the inner coil circuit and 4 A for the outer coil circuits. The baseline condition was the optimal operating condition for P5, resulting in the highest thrust of the magnitude of 78.0 mN, a current utilization efficiency of 52.0%, and a peak-to-peak discharge current oscillation of 52.5%. With the introduction of the magnetic field gradient, the magnitude of the gradient increased as the testing conditions progressed, resulting in a decrease in thruster performance, as illustrated in figure 5. The magnitude of the magnetic field in the localized region was reduced due to the reduction in current across the two independently operating coils. However, the area span across which the gradient was observed was also increased. As the magnitude of the azimuthal gradient grew, the thrust and efficiency of the thruster both dropped due to the higher magnitude. The instability is demonstrated by the peak-to-peak percentage of the discharge current—the higher the peak-to-peak percentage, the less stable the thruster operation. The percentage of peak-to-peak discharge current oscillation is estimated by observing the average peak to peak discharge current normalized over the operational discharge current recorded during thruster operation. The thruster operation became more unstable as the azimuthal gradient increased, increasing the peak-to-peak of the discharge current oscillation. The trends closely aligned with the uniform magnetic field test matrix outcomes. This variation in performance also indicated that a significant impact on performance was observed despite the gradient being very small compared to the magnetic field’s magnitude in the uniform portion of the channel.

By examining the performance change, it is evident in figure 5 that the magnitude of the magnetic field in the region of maximal gradient decreased by an average of 6 G across all operational conditions. Implementing the localized gradient led to an average reduction of 0.7 mN in thrust across all operational conditions, resulting in a 2.9% decrease from the baseline. Locally, the magnetic field experienced an average 4.4% decrease due to the gradients. As stated in the preceding section, the uncertainty associated with the thrust measurement is $\pm 2 \text{ mN}$. Therefore, the changes in thrust lie slightly beyond the uncertainty ranges, indicating a minimal impact of

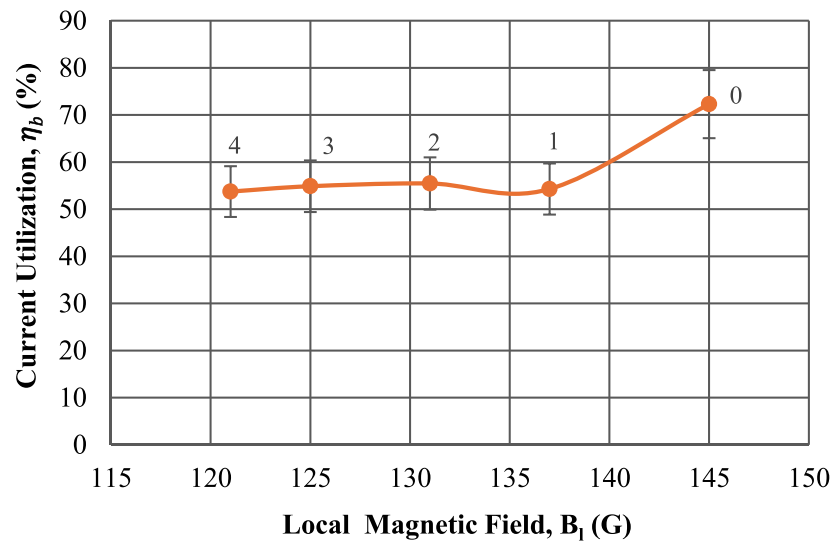
magnetic field shifts on thrust. Similarly, the specific impulse exhibited the same trend as the thrust, resulting in an average magnitude decrease of 12.3 s and a 2.9% decrease with a gradient in the magnetic field compared to the uniform condition. The current utilization efficiency experienced an average 4.6% decrease in magnitude for a 24.5% decrease with a gradient in the magnetic field compared to the baseline condition. Finally, the peak-to-peak percentage of the discharge current oscillation increased on average by 21.0% due to the gradient introduction. The azimuthal magnetic field gradient’s influence on thruster stability illustrated that the stability of thruster operation is one of the thruster performance parameters most significantly influenced by non-uniformity. To summarize the findings, the HET’s thrust decreased by 2.4 mN and 3.1% as the operation transitioned from the baseline to the one-coil-off condition i.e. test condition 2 or gradient 2. The efficiency also decreased by 23.3%, the peak-to-peak of the discharge current oscillations increased by 23.6%, and the magnetic field decreased by 9.7%. In the same way, the reduction of the magnetic field by 16.6% for two-coils-off condition i.e. test condition 4 or Gradient 4 resulted in a decrease of 2.73 mN and 3.5% in thrust, a 25.7% decrease in efficiency, and a 31.5% increase in the peak-to-peak discharge current oscillations.

5.2. Plasma processes associated with performance changes due to azimuthal magnetic field gradient

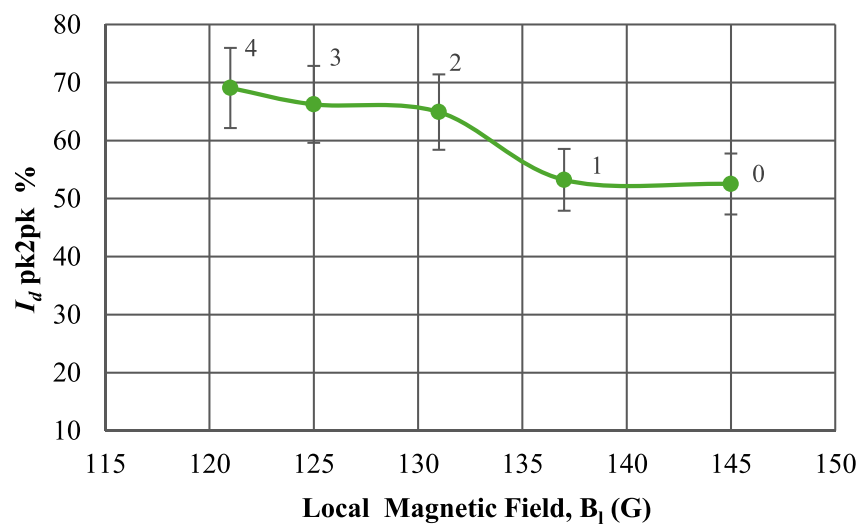
In light of the performance model, the magnetic field is a critical factor in influencing the ionization and acceleration processes. The impact of the magnetic field was translated into a change in plasma parameters and, consequently, the thruster’s performance. The model illustrates the impact of the azimuthal magnetic field on the performance parameters in the vicinity of the exit plane. The magnetic field experienced an azimuthal gradient due to the localized region’s loss of the magnetic field. The electron confinement in the channel decreases as the electrons transition from the high uniform magnetic field region to a sectional lower magnetic field region as a result of the gradient’s introduction in the HET channel as shown in figure 1. The lesser confinement of the electrons increases the electron flux in the gradient region. The reduction in confinement leads to a decrease in collision frequency, resulting in a decrease in ionization due to the reduced electron number density. Electrons undergo ohmic heating, leading to a decrease in temperature due to the decreased likelihood of ionization collisions. A decrease in the electron temperature results in a decrease in



a)



b)



c)

Figure 5. Variations of performance parameters as a function of local magnetic field (a) thrust (b) current utilization efficiency, and (c) pk-to-pk% of discharge current for azimuthal magnetic field gradient test conditions at 300 V, 5.61 mg s^{-1} anode and 0.44 mg s^{-1} cathode flow rates.

the energy possessed by the charged species, which leads to a less positive plasma potential at that location. Therefore, an azimuthal magnetic field gradient in the non-uniform operating condition results in a non-uniform distribution of the electron number density and electron temperature in the channel. The electron temperature decreases along with the collision frequency, decreasing the total energy the electrons acquire as they travel azimuthally. The drop in energy causes the electrons to travel upstream in the region of the azimuthal gradient to gather energy for ionization. This motion leads to a localized shift in the ionization acceleration region, which causes the region to move upstream towards the anode at the gradient's location. Consequently, the azimuthal gradient influences the ions, which are now formed further upstream within the localized region. The loss voltage is increased as a result of the increased likelihood of wall collisions and neutralization collisions among the ions. The acceleration voltage decreases due to the increase in the loss voltage for a fixed discharge voltage. The decrease in acceleration voltage indicates a decrease in ion velocity, which causes a change in efficiency, specific impulse, and thrust.

Further examination of the discharge current oscillation reveals that the electron motion can be characterized as a blend of thermal and kinetic energy. The kinetic energy of electrons increases, and thermal energy decreases as a result of a decrease in the magnetic field. In order to stabilize the discharge current oscillation, it is imperative to maintain the energy balance. The momentum transfer collision frequency decreases as the electrons propagate from the region of the high magnetic field to the low magnetic field, and the electron temperature decreases as a consequence of reduced ohmic heating. This variation leads to non-uniformities throughout the channel during ionization collisions. The imbalance between Joule heating and the convection term associated with wall loss caused by enhanced oscillation increases as the electrons drift in the azimuthal and axial direction. A decrease in thermal energy indicates a decrease in ionization collision and an increase in atom excitation collision. Therefore, the azimuthal gradient results in a general decrease in the ion beam current, leading to a decrease in the current utilization efficiency. Not only does the azimuthal gradient increase the mobility of electrons, but it also causes the gyroscopic frequency to fluctuate and increase in the region of the low magnetic field due to the variation of the magnetic field. The proper confinement of electrons in the axial and azimuthal directions is necessary to maintain or accomplish the stability of the HET, as shown by discharge current oscillation. The reduction in electron confinement affects the frequency of ionization collisions, and electron generation near the anode results in a non-uniform length of the ionization acceleration area, resulting in variations in electron number density across the channel. The collision frequency and electron production rate influence the discharge current oscillation, resulting in the non-stable operation of the HET, which attempts to maintain plasma discharge. The introduction of a gradient has the most significant impact on discharge current oscillation, as the magnitude of the magnetic field significantly influences electron motion and collision processes.

The results presented emphasize the change in plasma parameters at the far field despite the azimuthal gradient resulting in the highest reduction in the magnitude of the magnetic field, which is 16.6% of the baseline magnetic field. The model offers potential explanations for the processes taking place in the channel. The plume measurement serves as evidence of the significant influence of in-channel non-uniformities. Though in-channel measurements of plasma parameters will provide deeper insights regarding the plasma processes, the impact of the azimuthal magnetic field gradient on thruster performance is established in the current study using far-field measurements. The diagnostics were employed to conduct measurements to observe the far-field changes caused by the gradient. The experimental results demonstrated a reduction of 8.1% in electron temperature and a decrease of 5.1% in acceleration voltage compared to the baseline condition when one coil was turned off. Additionally, there was a decrease of 12.9% in electron temperature and a fall of 6.0% in acceleration voltage when two coils were turned off, as seen in figures 6 and 7. Examining the uncertainty linked to the Langmuir and RPA probe, there was a strong rationale for the capability to detect the impact of the azimuthal gradient on the plasma parameters. Figure 5 illustrates the model's validation of the thruster's efficiency in relation to the magnetic field. It is crucial to emphasize that the other magnetic circuit maintained sufficient operational stability to enable continuous thruster operation despite the thruster experiencing a decrease in stable operation due to the two coils in the circuit being off in the current study.

The azimuthal magnetic field gradient influenced the thruster performance in terms of magnitude and the plume's orientation as seen in figure 8. The position of the maximum ion current collected by the sweeping Faraday probe was monitored by utilizing the three-dimensional measurement of the ion current density acquired through the custom-designed Sweep Probe Apparatus. When a Faraday scan cannot pick up on the distinctive double peaks, the ion current density peak becomes a reliable indicator of the position of the thrust vector [24]. Table 4 displays the thrust vector's location for the baseline line condition and the varying azimuthal magnetic field gradient condition.

The thruster's inclination was measured during installation, and a vertically downward angular incline of 0.2° was determined. This inclination was 5% of the thruster vector value obtained for the baseline condition and, as a result, is disregarded in the current analysis. The thrust vector for the baseline condition was determined to be 0° horizontally and 4° vertically downward. The two coils, independently actuated, were situated on the right side of the thruster when viewed from the front, as illustrated in figure 3. The position of the thrust vector changed to 5° horizontally and 3° vertically when the OC2 circuit was off. The ion current density peak was deviated due to the magnetic field lines passing through the inner coil being modified due to the OC2 circuit being turned off and possibly tilted towards the outer coil rather than at the centerline location, which was probable for the magnetic field lines. The OC2 and OC3 circuits being off corresponded to the condition of two coils turned off. It is evident that the presence of a $0.04 \text{ G}/^\circ$ higher gradient, as opposed to a single coil

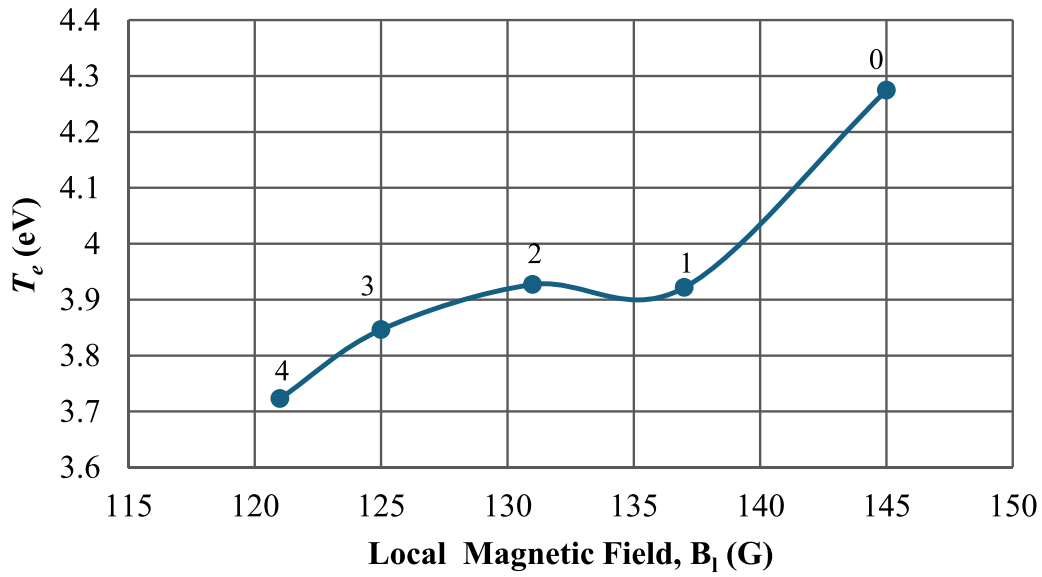


Figure 6. Electron temperature as a function of local magnetic field for azimuthal magnetic field gradient test matrix 2 test conditions at 300 V, 5.61 mg s^{-1} anode, and 0.44 mg s^{-1} cathode flow rates.

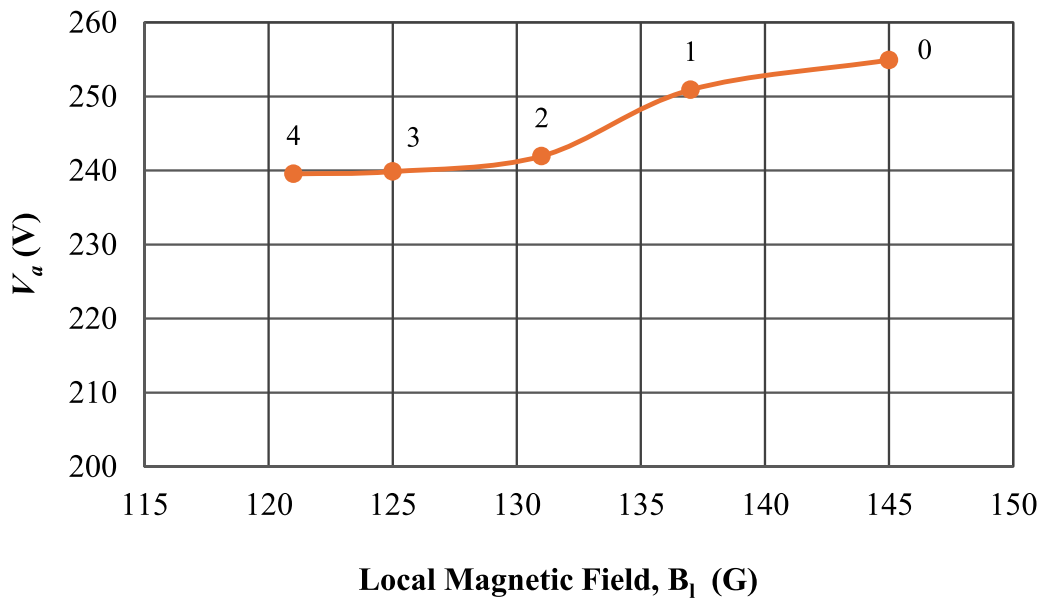


Figure 7. Ion acceleration voltage as a function of local magnetic field for azimuthal magnetic field gradient test matrix 2 test conditions at 300 V, 5.61 mg s^{-1} anode and 0.44 mg s^{-1} cathode flow rates.

being off, caused a 2° vertical deviation in the thrust vector. The magnetic field experienced a greater magnitude decrease due to the additional coil's turning off. Additionally, the gradient was able to traverse a larger area, resulting in a fluctuation in the vertical position of the peak. The current study provides the impact the introduction of azimuthal magnetic field gradient has on the far field plasma properties. To provide detailed measurements of properties inside the channel, future work is required to measure plasma parameters within the thruster channel to determine how local azimuthal magnetic

field changes affect these parameters. The measurement conducted within the channel with a gradient will establish correlations between the recorded plasma properties and the far field measurements observed during changes in the magnetic field. Observing the impact to a greater extent is possible by introducing a higher magnitude of the gradient, which can result in the HET operating at its maximal gradient. Future studies will be critical in qualifying thrusters for space flights by the commercial sector, which mass produces thrusters for space missions.

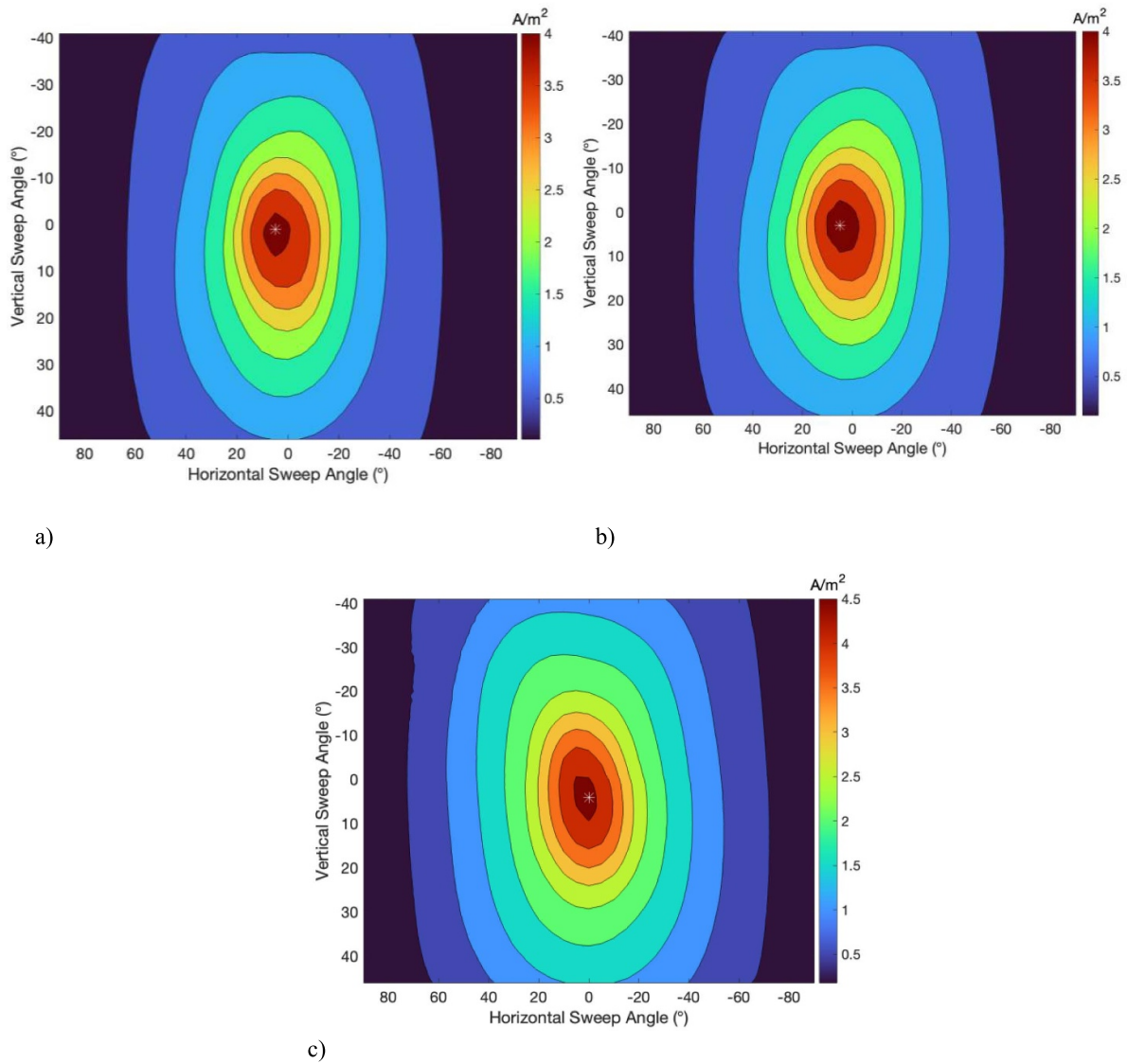


Figure 8. Contour map of ion current density using sweep probe apparatus for (a) baseline condition (b) test condition 2 representing ‘one coil off’ operation and (c) test condition 4 representing ‘two coils off’ condition. The thrust vector position is denoted by the asterisks on the contour plots.

Table 4. Thrust vector position for azimuthal magnetic field gradient test conditions at 300 V, 5.61 mg s⁻¹ anode and 0.44 mg s⁻¹ cathode flow rates. Test condition 2 or gradient 2 represents ‘one coil off’ operating condition and test condition 4 or gradient 4 represents ‘two coils off’ operating condition.

Test No.	Condition Name	B_r (G)	$\nabla_{\theta} B_r$ (G/°)	Horizontal (°)	Vertical (°)
0	Baseline	145	0.00	0	4
1	Gradient 1	137	0.18	5	2
2	Gradient 2	131	0.31	5	3
3	Gradient 3	125	0.30	5	3
4	Gradient 4	121	0.36	5	1

6. Conclusion

The primary objective of the study is to quantify the impact of incorporating an azimuthal magnetic field gradient on HET performance. To accomplish this objective, we divided the outer coil circuit into three segments: two independent coils

and six coils connected in series. By deactivating the electrical current flowing through the separate coils, a magnetic field with a varied magnitude was created in the channel, resulting in an azimuthal gradient. The azimuthal magnetic field gradient’s presence had the greatest impact on the stable operation of the thruster and the least on the thrust it generated.

In contrast to a 3.5% decrease in thrust, a 0.4 G/° gradient in the magnetic field leads to a 31.5% decrease in stability. As the magnitude of the azimuthal gradient of the magnetic field increased, the current utilization efficiency was most significantly impacted and contributed significantly to the overall efficiency decrease. It is also important to note that the thruster continued to operate without shutting down, even though two coils were off, resulting in the peak-to-peak percentage of discharge current oscillations of 69.1%. The study provides an understanding of the impact of the presence of azimuthal magnetic field gradient on the thruster performance. This analysis offered a perspective on the close drift of electrons, a critical principle that should be employed in developing thrusters to ensure that they operate reliably. It was established that the presence of an azimuthal magnetic field gradient contributed to a decrease in the thruster stability and efficiency. Through the physics-based performance model proposed in the study, the impact of azimuthal magnetic field gradient on the electron parameters, such as the electron temperature is established. The model establishes the impact of electron temperature on the motion of the charged particles. The effect of the motion of the electrons on the plasma properties measured far field, as well as the performance parameters such as efficiency and thrust, is established through this study. Through the current work, we contributed significantly to understanding the impact of non-uniformities in the azimuthal magnetic field gradient on the thruster's performance, specifically regarding efficiency, thrust, and stability.

Data availability statement

All data that support the findings of this study are included within the article (and any supplementary files).

Acknowledgments

The authors acknowledge the resources provided by the High-Power Electric Propulsion Laboratory of the Georgia Institute of Technology for conducting this work. The authors declare there is no conflict of interest. No funding was used for the study. Chhavi conceptualized the study, conducted the experiments and analysed the data. Chhavi Chhavi wrote the manuscript with input from all authors. Mitchell Walker provided guidance along the study. All authors read and approved the final manuscript. The authors knowledge that Chhavi Chhavi is an inventor on the U.S. Patent No. US 12,322,581 B1 which is related to the technology discussed in the paper.

ORCID iD

Chhavi Chhavi  0009-0009-3327-3906

References

- [1] Goebel D M and Katz I 2008 *Fundamentals of Electric Propulsion: Ion and Hall Thrusters* (Wiley) (<https://doi.org/10.1002/9780470436448>)
- [2] Hofer R and Gallimore A 2006 High-specific impulse Hall thrusters, part 2: efficiency analysis *J. Propul. Power* **22** 732–40
- [3] Lev D, Myers R M, Lemmer K M, Kolbeck J, Koizumi H and Polzin K 2019 The technological and commercial expansion of electric propulsion *Acta Astronaut.* **159** 213–27
- [4] O'Reilly D, Herdrich G and Kavanagh D F 2021 Electric propulsion methods for small satellites: a review *Aerospace* **8** 22
- [5] Bapat A, Salunkhe P B and Patil A V 2022 Hall-effect thrusters for deep-space missions: a review *IEEE Trans. Plasma Sci.* **50** 189–202
- [6] Misuri T, Pergola P and Andrenucci M 2013 HT5k Hall thruster to improve small launcher capabilities *IEPC Paper* pp 2013–279
- [7] Raitses Y, Guelman M, Ashkenazy J and Appelbaum G 1999 Orbit transfer with a variable thrust Hall thruster under drag *J. Spacecr. Rockets* **36** 875–81
- [8] Jackson J, Cassady J, Allen M, Myers R, Tofil T A, Herman D A and Pencil E J 2018 Development of high power Hall thruster systems to enable the NASA exploration vision *Space Propulsion Conf. Paper* pp 2018–429
- [9] Victor A L, Zurbuchen T H and Gallimore A D 2006 Ion-energy plume diagnostics on the BHT-600 Hall thruster cluster *J. Propul. Power* **22** 1421–4
- [10] Beal B E, Gallimore A D, Haas J M and Hargus W A 2004 Plasma properties in the plume of a Hall thruster cluster *J. Propul. Power* **20** 985–91
- [11] Hall S J, Jorns B A, Cusson S E, Gallimore A D, Kamhawi H, Peterson P Y, Haag T W, Mackey J A, Baird M J and Gilland J H 2022 Performance and high-speed characterization of a 100-kW nested Hall thruster *J. Propul. Power* **38** 40–50
- [12] Liang R 2013 The Combination of Two Concentric Discharge Channels into a Nested Hall-Effect Thruster *PhD Dissertation* Aerospace Engineering Department, University of Michigan
- [13] Duchemin O and Valentian D 2007 Thrust vector control using multi-channel hall-effect thrusters *AIAA J.* pp 2007–5203
- [14] Hofer R R 2004 Development and characterization of high-efficiency, high-specific impulse xenon Hall thrusters *PhD Dissertation* Aerospace Engineering Department, University of Michigan
- [15] Komurasaki K and Arakawa Y 1992 Hall current ion-thruster performance *J. Propul. Power* **8** 1212–6
- [16] Kim V 1998 Main physical features and processes determining the performance of stationary plasma thrusters *J. Propul. Power* **14** 736–43
- [17] Hofer R and Jankovsky R 2001 A Hall thruster performance model incorporating the effects of a multiply-charged plasma *AIAA J.* pp 2001–3322
- [18] Ding Y, Li P, Zhang X, Wei L, Sun H, Peng W and Yu D 2017 Effects of the magnetic field gradient on the wall power deposition of Hall thrusters *J. Plasma Phys.* **83** 905830205
- [19] Morozov A I, Esipchuk Y V, Kapulkin A M, Nevrovskii V A and Smirnov V A 1972 Effect of the magnetic field on a closed-electron drift accelerator *Sov. Phys. Tech. Phys.* **17** 482–7 (available at: www.osti.gov/biblio/4654554)

- [20] Gao Y, Wang W, Xue S, Li Y and Cai G 2022 Influence of the upstream axial magnetic mirror field on the plume characteristics in the full cylindrical Hall thruster *Acta Astronaut.* **196** 186–93
- [21] Jiang Y, Tang H, Ren J, Li M and Cao J 2018 Magnetic mirror effect in a cylindrical Hall thruster *J. Phys. D: Appl. Phys.* **51** 035201
- [22] Keidar M and Boyd I D 2005 On the magnetic mirror effect in Hall thrusters *Appl. Phys. Lett.* **87** 121501
- [23] Daren Y, Hui L and Haiyang F 2009 Effect of magnetic mirror on the asymmetry of the radial profile of near-wall conductivity in Hall thrusters *Plasma Sci. Technol.* **11** 1–7
- [24] Kornberg O 2007 Investigation of magnetic field profile effects in Hall thrusters *Master of Science Dissertation* Embry-Riddle Aeronautical University—Daytona Beach
- [25] Peterson P, Gallimore A and Haas J Experimental investigation of Hall thruster internal magnetic field topography *AIAA-2001-3890 Presented in 37th Joint Propulsion Conf. and Exhibit* (<https://doi.org/10.2514/6.2001-3890>)
- [26] Harvey M L 2014 The effect of the 2-Dimensional magnetic field profile in Hall thrusters *Master of Science Dissertation* Embry-Riddle Aeronautical University—Daytona Beach
- [27] Yang L, Wang P Y and Wang T 2023 Study on the Influence of magnetic field on the performance of a 5 kW hall thruster *Front. Mater.* **10** 1150802
- [28] Garrigues L, Hagelaar G J M, Bareilles J, Boniface C and Boeuf J P 2003 Model study of the influence of the magnetic field configuration on the performance and lifetime of a Hall thruster *Phys. Plasmas* **10** 4886–92
- [29] Fan H, Xu Y, Wang L, Wei L, Li H, Guo N and Ding Y 2022 Effects of unsymmetrical magnetic field on discharge characteristics of Hall thruster with large height-radius ratio *Vacuum* **203** 111261
- [30] Reid B M and Gallimore A 2007 Review of hall thruster neutral flow dynamics *IEPC Paper* pp 2007–38
- [31] Benavides G F *et al* 2019 Development of a high-propellant throughput small spacecraft electric propulsion system to enable lower cost NASA science missions *AIAA Paper* pp 2019–4162
- [32] Lazurenko A, Kim V, Bishaev A and Auweter-Kurtz M 2005 Three-dimensional simulation of atom and ion dynamics in a stationary plasma thruster *J. Appl. Phys.* **98** 043303
- [33] Mazouffre S, Bourgeois G, Vaudolon J, Garrigues L, Hénaux C, Harribey D, Vilamot R, Rossi A, Zurbach S and Le Méhauté D 2015 Development and testing of hall thruster with flexible magnetic field configuration *J. Propul. Power* **31** 1167–74
- [34] Gulczynski F 1999 Examination of the structure and evolution of ion energy properties of a 5 kw class laboratory Hall effect thruster at various operational conditions *PhD Dissertation* Aerospace Engineering Department, University of Michigan
- [35] Daren Y, Yongjie D and Zhi Z 2005 Improvement on the scaling theory of the stationary plasma thruster *J. Propul. Power* **21** 139–43
- [36] Yamamoto N, Komurasaki K and Arakawa Y 2006 Erratum for ‘discharge current oscillation in Hall thrusters,’ *J. Propul. Power* **22** 478
- [37] Kieckhafer A W 2011 Recirculating liquid nitrogen system for operation of cryogenic pumps *IEPC Paper* pp 2011–217
- [38] Dushman S 1949 *Scientific Foundations of Vacuum Technique* (Wiley)
- [39] Haas J M and Gallimore A D 2001 Internal plasma potential profiles in a laboratory-model Hall thruster *Phys. Plasmas* **8** 652–60
- [40] Chhavi C and Walker M Three—dimensional sweep probe system *U.S. Patent No. 12,322,581* U.S. Patent and Trademark Office (available at: <https://ppubs.uspto.gov/api/patents/html/12322581>)
- [41] Frieman J D, Brown N P, Liu C Y, Liu T M, Walker M L R, Khayms V and King D Q 2018 Electrical facility effects on faraday probe measurements *J. Propul. Power* **34** 267–9
- [42] Brown D L, Walker M L R, Szabo J, Huang W and Foster J E 2017 Recommended practice for use of faraday probes in electric propulsion testing *J. Propul. Power* **33** 582–613
- [43] Lobbia R B and Beal B E 2017 Recommended practice for use of Langmuir probes in electric propulsion testing *J. Propul. Power* **33** 566–81
- [44] Hofer R and Gallimore A 2023 Ion species fractions in the far-field plume of a high-specific impulse Hall thruster *AIAA Paper* pp 2003–5001